Modulating the Enantiodiscrimination Features of Inherently Chiral Selectors by Molecular Design: A HPLC and Voltammetry Study Case with Atropisomeric 2,2′-Biindole-Based Monomers and Oligomer Films

Luca Scapinello[+],[a] Sara Grecchi[+],[b] Sergio Rossi,[b] Fabiana Arduini,[c] Serena Arnaboldi,[b] Andrea Penoni,[a] Roberto Cirilli,*[d] Patrizia Romana Mussini,*[b] and Tiziana Benincori*[a]

Abstract: A family of inherently chiral electroactive selectors based on the 2,2′-biindole atropisomeric scaffold, of easy synthesis and modulable functional properties, is studied in cascade in two enantioselection contexts. They are at first investigated as probes in enantioselective HPLC, studying molecular structure and temperature effects, and achieving very efficient semipreparative enantioseparation. The enantiomers thus obtained, of remarkable chiroptical features (optical rotation as well as circular dichroism), are successfully applied as selectors in chiral voltammetry in different media for discrimination of the enantiomers of chiral electroactive probes, either by conversion into enantiopure electroactive electrode surfaces by electrooligomerization on glassy carbon substrate (the two monomers with shorter alkyl chains), or as chiral additive in achiral ionic liquid (the monomer with longest alkyl chains). Discrimination is conveniently and reproducibly achieved in terms of significant potential differences for the two enantiomers, specularly inverting either probe or selector configuration. In one case successful discrimination is also observed with the two probe enantiomers concurrently present, either as racemate or with enantiomeric excesses, neatly accounted for by the peak current ratios.

Introduction

Recently, outstanding enantiodiscrimination has been achieved in chiral electroanalysis, chiroptics and magnetoelectrochemistry experiments employing as chiral selectors electroactive oligomer films electrodeposited from 3,3′-bis(2,2′-bithiophen-5-yl)-1,′dimethyl-1*H*,1′*H*-2,2′-biindole (**N-Me-IND)$_2$-T$_4$** in Figure 1).[1]

Such performances can be ascribed to the "inherent chirality" of the monomer and related oligomers. This property implies chirality and key functional properties to originate from the same element, corresponding in this case to the whole main conjugated backbone of the molecule, featuring a torsion associated to a racemization barrier too high to be overcome at room temperature.[2] Inherent chirality, typical of atropisomeric and helical chiral selectors, results in huge chirality manifestations in both chiroptics[3,4] and chiral electrochemistry[2,5] and

[a] *Dr. L. Scapinello,[+] Prof. A. Penoni, Prof. T. Benincori*
Dipartimento di Scienza e Alta Tecnologia
Università degli Studi dell'Insubria
Via Valleggio 11, 22100 Como (Italy)
E-mail: tiziana.benincori@uninsubria.it

[b] *S. Grecchi,[+] Dr. S. Rossi, Dr. S. Arnaboldi, Prof. P. Romana Mussini*
Dipartimento di Chimica
Università degli Studi di Milano
Via Golgi 19, 20133 Milano (Italy)
E-mail: patrizia.mussini@unimi.it

[c] *Prof. F. Arduini*
Dipartimento di Scienze e Tecnologie Chimiche
Università di Roma Tor Vergata
Via della Ricerca Scientifica, 100133 Roma (Italy)

[d] *Dr. R. Cirilli*
Centro Nazionale per il Controllo e la Valutazione dei Farmaci
Istituto Superiore di Sanità
Viale Regina Elena 299, 00161 Roma (Italy)
E-mail: roberto.cirilli@iss.it

[+] *These authors contributed equally to this work.*

Supporting information for this article is available on the WWW under https://doi.org/10.1002/chem.202101170

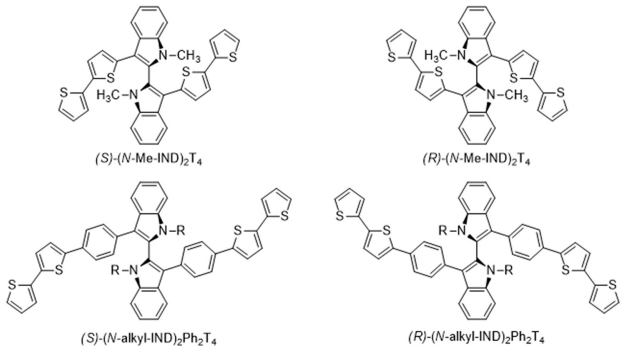

Figure 1. The parent 2,2′-biindole monomer **(N-Me-IND)$_2$-T$_4$**[1] and the systematic monomer subfamily investigated in the current study (R═Me (**1**), Pr (**2**), *n*-Hex (**3**)).

also implies the possibility of fine, reversible electrochemical modulation of chiroptics features.[6]

Of outstanding impact for electroanalytical applications is the fact that implementing inherently chiral selectors at the electrode-solution interphase, either at the electrode surface[7] or in the medium,[8] the enantiomers of many electroactive chiral probes, including pharmaceutically interesting ones, can be neatly discriminated in chiral voltammetry experiments in terms of large differences in peak potentials, the most convenient transduction mode. In fact, unlike the case of for example current or conductivity differences, it can enable direct enantiomer identification (with possible concurrent quantification from the peak current) as well as selective enantiomer electrochemical activation.[5]

Focusing on atropisomeric selectors, attractive enantiodiscrimination performances have been observed with 3,3′-bibenzothiophene,[6,9] 3,3′-bithiophene[10] and 1,1′-binaphthyl[11] systems, besides the above 2,2′-biindole one.[1,12] However, biindole systems offer a peculiar important advantage, namely, very easy modulation of functional properties through easy design tuning. In fact, their synthesis can be easily adapted to modulate the structure of the monomer terminals; moreover, their *N* atoms can be easily functionalized with alkyl chains of different lengths (an effective tool to tune, for instance, solubility and processability), or even more complex substituents with specific properties.

In this context, a systematic study case is now proposed, based on a 2,2′-biindole series **(N-R-IND)$_2$-Ph$_2$T$_4$** (**1**, **2**,[12] and **3** in Figure 1 with R = methyl, n-propyl or n-hexyl, respectively) featuring systematic variation of the N alkyl substituents of the pyrrolic rings in the core, besides a modification on the terminals[12] with respect to the above parent case **(N-Me-IND)$_2$-T$_4$**,[1] of concern for applicative issues, like modulating enantiomer separability in enantioselective HPLC, as well as fundamental issues, like the localization of the HOMO and LUMO orbitals with related implications for the selector chiroptical and redox features.

The family is studied in cascade in two enantioselection contexts:

- as probes, in enantioselective HPLC, studying molecular structure and temperature effects and achieving very efficient semipreparative enantioseparations;
- as selectors, in chiral voltammetry, testing as a function of molecular structure the enantiopure antipodes, obtained in the former HPLC step, for discrimination of the enantiomers of chiral electroactive probes, either by conversion into enantiopure electroactive electrode surfaces by electrooligomerization on glassy carbon GC substrate, or as chiral additives in achiral ionic liquid, according to an alternative enantiodiscrimination strategy also recently developed.[8,13]

Results and Discussion

Synthesis of inherently chiral monomers 1–3

The synthesis of the family of chiral selectors **1**–**3** was performed following a modified Larock protocol[13] allowing the formation in one step both of the interannular bond between the two indole moieties and their functionalization in the 3,3′-positions, although in modest yield.

The 2,2′-biindole intermediate **6** was obtained in 36% yield by reacting the butadiine **4**[15,16] and the 5-(4- bromophenyl)-2,2′-bithiophene[17] (**5**) in the presence of tetrakis (triphenylphosphine)palladium(0) as catalyst and K_2CO_3 as a base in refluxing acetonitrile. The alkylation of the nitrogen atoms with the suitable haloderivative in the presence of KOH in DMF solution afforded compounds **1**–**3** in good yield (Scheme 1).

HPLC separation of enantiomers of 1–3, and absolute configuration assignment

The next step was achieving multimilligram amounts of enantiopure antipodes of each chiral monomer, necessary to prepare enantiopure electrode surfaces by electrooligomerization; this required the development of efficient *ad hoc* enantioselective HPLC protocols. To this aim, an accurate study on the enantioseparation ability of the analytical 250 mm × 4.6 mm, 5 μm, Chiralpak IB column was carried out.

Different ternary mobile phases were evaluated, containing

- a hydrocarbon (*n*-hexane)
- an alcohol (ethanol or isopropanol)
- a solvent capable of solubilizing the chiral analytes (such as dichloromethane or acetone).

In each elution condition, the column temperature was changed from 5 to 45 °C, in 10 °C increments.

The best results in terms of enantioselectivity were obtained using as mobile phases the mixtures

- *n*-hexane/EtOH/dichloromethane 100:1:5 (v/v/v), i.e. the same employed for enantioseparation of the parent monomer ,[1] at 25 °C), and
- *n*-hexane/EtOH/acetone 100:1:5 (v/v/v).

Table 1 reports the experimental values at 5 °C in the two above eluents of retention factors k_1 for the first eluted enantiomer of compounds **1**–**3** (at such temperature the (*S*)-one in all cases), as well as of related enantioseparation factors $\alpha = k_2/k_1$.

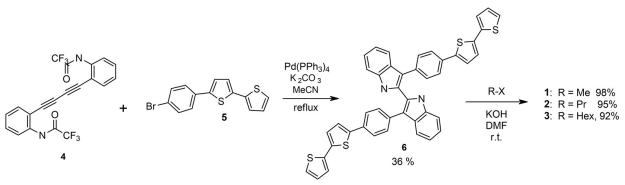

Scheme 1. General strategy for the synthesis of monomers **1**–**3**.

Table 1. Retention and enantioseparation factors, thermodynamic data and isoenantioselectivity temperatures pertinent to the enantiodiscrimination of **1–3** on the Chiralpak IB CSP with two selected ternary mobile phases.

Compound	Mobile phase	k_1 (AC)[a]	α (5 °C)	$\Delta\Delta S°$ (u.e.)	$\Delta\Delta H°$ (kcal/mol)	T_{iso} (°C)
1	*n*-Hexane/EtOH/CH_2Cl_2 100:1:5	4.60 (*S*)	1.77	−5.97	−1.97	56.9
2		2.49 (*S*)	1.94	−7.09	−2.34	56.5
3		1.79 (*S*)	1.74	−6.88	−2.21	48.2
1	*n*-Hexane/EtOH/acetone 100:1:5	5.95 (*S*)	1.14	−2.19	−0.69	39.6
2		2.82 (*S*)	1.36	−3.55	−1.16	54.8
3		1.81 (*S*)	1.31	−3.89	−1.24	44.8

[a] Absolute configuration. Chromatographic conditions: Column, Chiralpak IB (250 mm×4.6 mm i.d.); mobile phase, as indicated in table; column temperature, 5 °C; flow rate, 1.0 mL/min; detection, UV at 380 nm.

Figure 2 displays the simultaneous resolution of 1–3 obtained on the Chiralpak IB CSP using *n*-hexane/EtOH/dichloromethane 100:1:5 (v/v/v) as mobile phase and monitoring simultaneously absorption and CD during chromatography.

As highlighted in Figure 2, at the lowest temperature of the range investigated,

i) the enantiomer (*S*) is always eluted before the (*R*) one;
ii) the retention of the (*S*)-enantiomer of the chiral analyte **3** with hexyl portion is lower than that of the homologues **1** or **2** with shorter alkyl chains;
iii) the peak pertinent to the second eluted enantiomer is unusually higher and narrower than the less retained one.

Furthermore, according to the enantioseparation factor values showed in Table 1, the chiral resolving ability of Chiralpak IB CSP decreased when replacing CH_2Cl_2 with acetone as organic modifier in mobile phase.

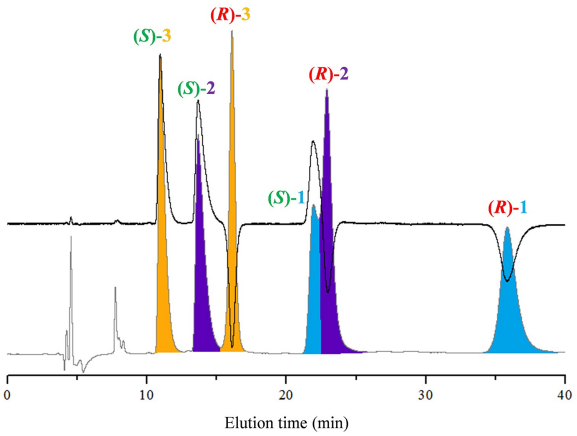

Figure 2. Simultaneous separation of compounds **1–3** on analytical 250 mm x 4.6 mm, 5 µm, Chiralpak IB column. Chromatographic conditions: mobile phase, *n*-hexane-dichloromethane-EtOH 100:5:1; column temperature, 5 °C; flow rate, 1 mL/min; detector, UV (grey) and CD (black) at 380 nm.

Experimental retention factors *k* for each compound enantiomer were correlated to the column temperature by van't Hoff analysis (Refs. [18–21], Supporting Information). Classical linear decreasing trends with the column temperature were obtained (Figure 3), pointing to a unique interaction mechanism governing the HPLC retention over the temperature range studied, and enabling estimation of $\Delta\Delta H°$ and $\Delta\Delta S°$ values for each molecule and eluent, which are collected in Table 1, too. In all cases they are negative, implying that *i*) the enantiorecognition of **1–3** results as a compromise between the favorable enthalpic contribution and unfavorable entropic contribution; *ii*) it exists an isoenantioselective temperature (T_{ISO}), defined as $T_{ISO}=\Delta\Delta H°/\Delta\Delta S°$ at which enthalpy-entropy compensation occurs and the enantiomers coelute (i.e. $\alpha=1$).[22–24] Thus, although the Chiralpak IB CSP is potentially able to separate the enantiomers of **1–3**, when the column temperature is set close to the T_{ISO} the two enantiomers coelute and no enantiodiscrimination should be observed (a single merged peak in correspondence of the intersection of the van 't Hoff retention plots is expected). Furthermore, above the crossover temperature the elution order of the enantiomers should be reversed. Notably, since the $\Delta\Delta H°$ and $\Delta\Delta S°$ values determine the magnitude of T_{ISO}, the enantiomer elution order of **1–3** as well as the enantioseparation ability of the Chiralpak IB, at a certain column temperature, critically depends on mobile phase composition. In the case of the eluent with dichloromethane cosolvent, such T_{ISO} values (Table 1) are well above the working temperature, pointing to the resolutions being always under enthalpy control ($|T_{ISO}\Delta\Delta S°| < |\Delta\Delta H°|$). Instead substitution of dichloromethane with acetone as the organic modifier in the mobile phase results in lower T_{ISO} values (intersection of the two enantiomer van't Hoff straight lines in the working *T* range in Figure 3), and the above inversion effect can be observed.

With the mobile phase *n*-hexane/EtOH/acetone 100:1:5 (v/v/v), increasing the temperature within enthalpic domain the chiral separation of all compounds deteriorated, and, whereas in the case of **2** the enantioseparation was always observable, the enantiomers of **1** and **3** coeluted at 35 °C and 45 °C, respectively, due to the proximity to the isoenantioselectivity conditions (Figures 3 and 4).

Above the cryptoenantioselectivity region a peak splitting and reversal of enantiomer elution order of **1** was clearly visible (i.e. the (*R*)-enantiomer was eluted before than (*S*)-enantiomer).

Such phenomenon was even more evident when replacing in the mobile phase ethanol with 2-propanol, resulting in a substantial decrease of T_{ISO} for all compounds (Table 1). In particular, with the mixture *n*-hexane/2-propanol/acetone 100:1:5 (v/v/v) the computed temperature of isoelution value falls always within the studied temperature range. Thus, the resolution is either under enthalpic and entropic control depending on column temperature, i.e. before T_{ISO} is enthalpy-driven and above T_{ISO} entropy-driven. Below T_{ISO} the enantioseparation factor decreases with temperature; close to T_{ISO} the recognition ability of the Chiralpak IB CSP disappears;[24,25] above T_{ISO}, the elution order of enantiomers swaps and the enantioseparation factor increases with increasing temperature (Figure 4). Having established the optimal experimental conditions for the

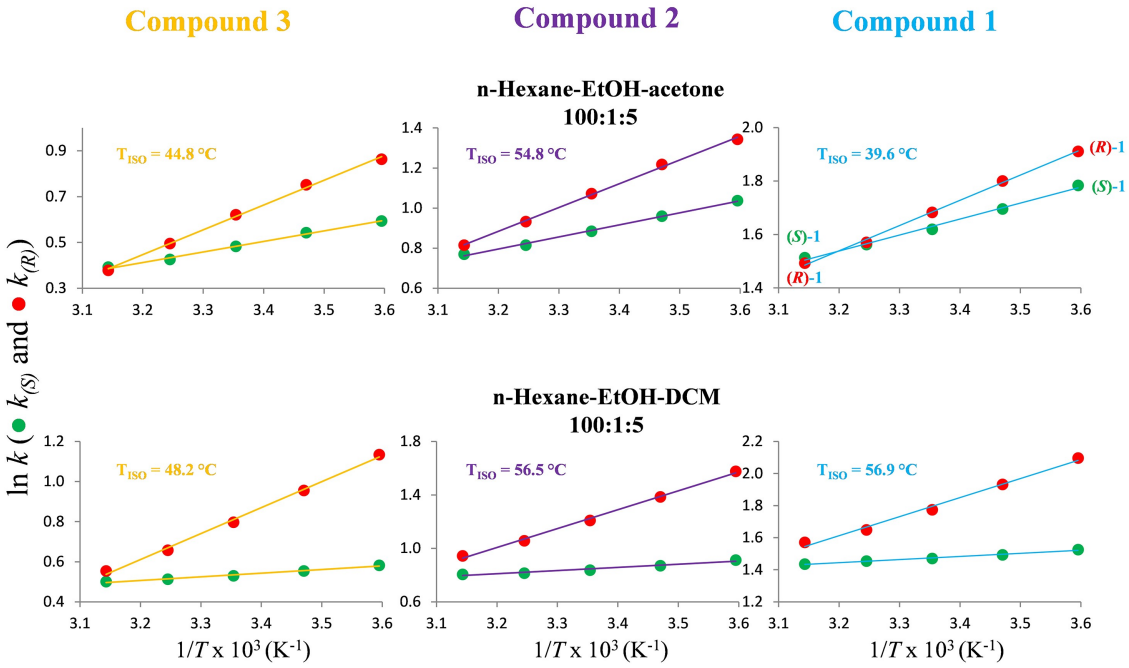

Figure 3. A comparison of van't Hoff plots (ln k vs. $1/T\times10^3$ according to van't Hoff equation ln $k=-\Delta H°/RT+\Delta S°/R+\ln\phi$) for the (*S*) and (*R*) enantiomers of compounds **1**–**3** on Chiralpak IB CSP. Chromatographic conditions: Column, Chiralpak IB (250 mm×4.6 mm i.d.); mobile phase, as indicated in figure; column temperature, 5–45 °C; flow rate, 1.0 mL/min; detection, UV at 380 nm.

HPLC resolution of **1**–**3** (mobile phase = *n*-hexane/EtOH/dichloromethane 100:1:5 and column temperature = 5 °C) the next step was to scale up them on a semipreparative scale using the 250 mm×10 mm I.D. Chiralpak IB column.

The good solubility of biindole compounds in the dichloromethane-based mobile phase as well as the high enantiodiscrimination ability of the Chiralpak IB CSP were key factors that made it possible to load onto the column mg amounts (from 5 to 10 mg) of racemic sample in a single run and obtain baseline enantioseparations. As an example Figure 5 shows the single-run HPLC resolution of 6 mg of racemic **3**. The enantiomeric excess of the two collected fractions was, for all compounds, >99%, and the yields of the enantiomeric separations ranged between 75% and 90%.

The CD spectra of the isolated enantiomers in chloroform solution between 500 and 230 nm were recorded (Figure 6). As expected, the CD curves of enantiomers were perfectly specular and their optical activity values (Table 2) were outstanding, in accordance with the presence in the molecules of an inherently dissymmetric chromophore.

In all cases, the first eluted enantiomer (green curves), showed a positive Cotton effect and it was dextrorotatory in chloroform solution. Same CD profile (Figure 5) and optical activity were recorded for the less retained enantiomer on the Chiralpak IB CSP of the chiral analogue **(N-Me-IND)$_2$-T$_4$**, devoid of the phenyl portion, whose absolute configuration was determined as (*S*) in a previous work.[1]

In summary, looking at Table 2 and Figure 6 the chiroptical features are, as expected,[26] dominated by the "exciton coupling chirality" features of the atropisomeric scaffold, i.e. a remarkable Davidov splitting effect resulting from the chiral molecule moieties behaving as two equivalent and reciprocally interacting chromophores,[3,4] with very little modulation from variations in either terminals or *N* alkyl substituents.

Table 2. Specific rotations of **1**–**3** in chloroform solution.[a]

	(*S*)-1	(*R*)-1	(*S*)-2	(*R*)-2	(*S*)-3	(*R*)-3
$[\alpha]^{20}_{589}$	1101	−1096	993	−990	970	−968

[a] Concentration: about 0.2 g/100 cm^3.

Monomer redox properties

The monomer characterization is an important preliminary step towards inherently chiral oligomer films. Redox features of the monomers were studied by cyclic voltammetry, also supported by DFT calculations (detailed results and discussion in chapter SI.2 in the Supporting Information), taking as benchmark the prototype case of parent monomer **(N-Me-IND)$_2$-T$_4$** in the same conditions.[1]

A peculiarity of 2,2′-biindole monomers[1,12] is that, unlike other atropisomeric monomer families so far studied,[6,9–11] first oxidations are typically localized mostly in the monomer core, on the two very electron rich pyrrolic units behaving as two equivalent reciprocally interacting redox centers. As a consequence, a twin first oxidation peak system is observed in

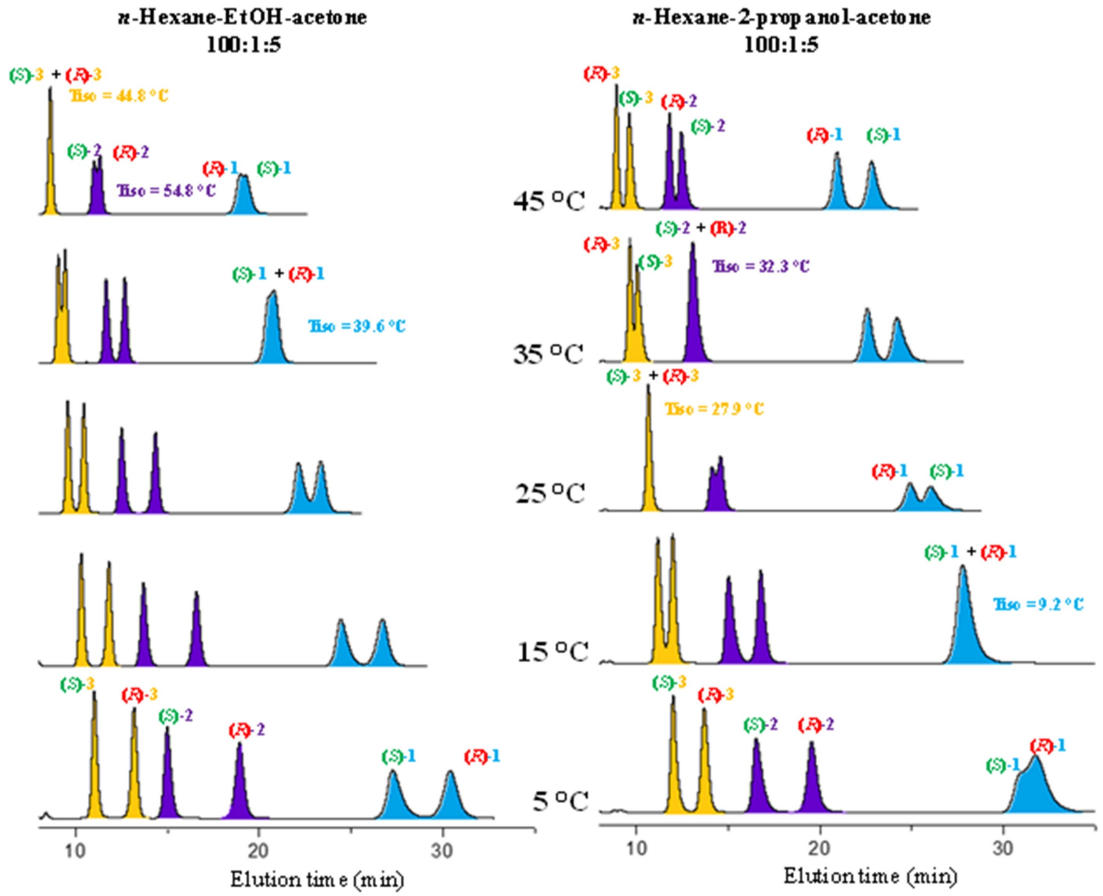

Figure 4. Temperature and alcohol cosolvent effect on T_{ISO} (and relevant inversion of enantiomer elution order) when eluting compounds **1**–**3** on Chiralpak IB column. Chromatographic conditions: Column, Chiralpak IB (250 mm × 4.6 mm i.d.); mobile phase, as indicated in figure; column temperature, as indicated in figure; flow rate, 1.0 mL/min; detection, UV at 380 nm.

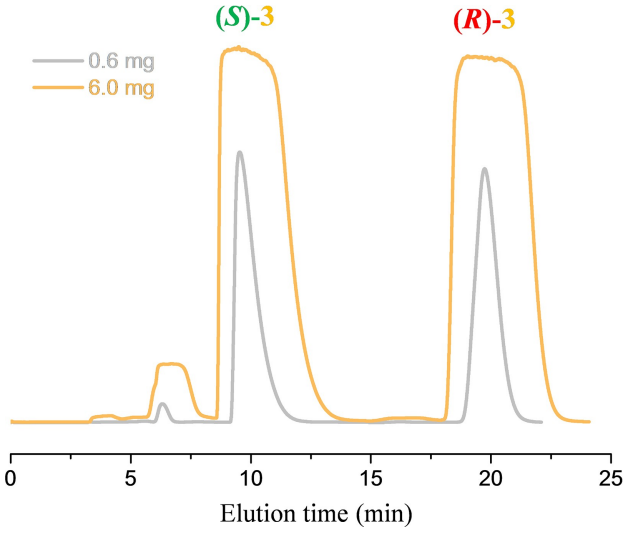

Figure 5. Semipreparative HPLC separation of (*S*)-**3** and (*R*)-**3** enantiomers. Chromatographic conditions: Column, Chiralpak IB (250 mm × 10 mm i.d.); mobile phase, *n*-hexane-dichloromethane-EtOH 100:5:1 (v/v/v); flow rate, 5.0 ml/min; temperature, 5 °C; detector, UV at 380 nm.

voltammetry,[27] of reversible character since the radical cations resulting from oxidation are stable being too far from the monomer terminals to give coupling. For this reason, oligomerization to yield chiral films on the electrode surface can only be achieved by a further oxidation process occurring at more positive potentials and localized on the monomer terminals.[1,12] Interestingly, in the parent case[1] theoretical computations showed that at least the thiophene rings adjacent to the core are significantly involved in the HOMO together with the pyrrole rings. On the other hand, phenyl spacers have been reported to scarcely contribute to, or even hamper, global effective conjugation in heteroaromatic-based conjugated systems.[12,28–30] Thus a phenyl spacer could better define localization of the "internal" first oxidation and "peripheral" second oxidation processes of the inherently chiral monomer.

Normalized CV patterns recorded at 0.2 V/s scan rate in CH_2Cl_2 and CH_3CN for the three monomers **1**, **2** and **3** are collected in Figure 7 and relevant key parameters are summarized in Table 3 while more details are provided in chapter SI.3 in the Supporting Information. Comparing them with the parent compound ones,[1]

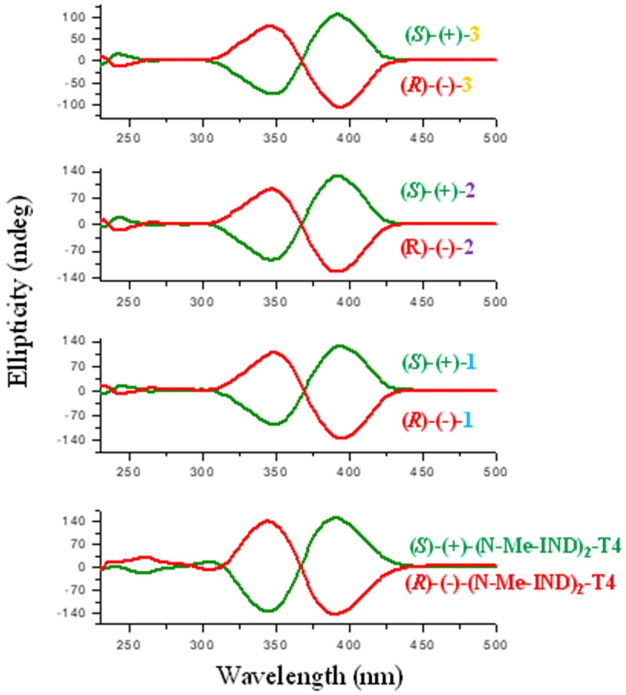

Figure 6. CD spectra of the antipodes of **1**–**3** and **(N-Me-IND)$_2$T$_4$** [1].

(*i*) also the present series features the above peculiar first oxidation twin reversible peak system in CH_2Cl_2, resulting in no chemical follow up, consistently with localization of first oxidations on the two pyrrolic moieties of the molecule core;[1,12]

(*ii*) and, again, the same twin processes tend to merge in CH_3CN,[1] since the polar solvent hampers reciprocal interactions between the interacting redox centers; moreover, they tend to become chemically irreversible at low scan rates, pointing to a chemical follow up;

(*iii*) in CH_3CN, enabling observation of reduction processes, too (unlike in CH_2Cl_2 where the reduction window is too narrow), the potentials for first reduction onset are similar to the parent case.

However, comparing the oxidative pattern in CH_2Cl_2 of parent **(N-Me-IND)$_2$-T$_4$** with the **1** one (Figure SI.3a), the first oxidation twin system involving the atropisomeric core looks remarkably shifted (by about 0.2 V) to more positive potentials with respect to the parent monomer (and even more for **2**[12] and **3**); in CH_3CN such shift is very small, but increases for **2** and **3**. This feature is consistent with the lower HOMO values obtained in DFT calculations for the present series respect to the parent monomer (Figure SI.2 top). The easier oxidation of the core in the parent monomer could be explained with the above mentioned significant involvement of the adjacent thiophene ring,[1] a feature that in the present series might be instead hampered by the phenyl group, possibly acting more as a spacer than as a linker (i.e. a contributor to the conjugation of the adjacent oligoheteroaromatic systems), confirming the above assumption supported by literature.[12,28–30] On the other hand, the nearly constant first reduction potentials look consistent with the LUMO being localized on the bithiophene terminals with small contribution from the phenyl spacer. They are also consistent with the nearly constant calculated LUMO values at least in three out of four cases (Figure SI.2 top); and actually also the fourth case could be considered in line, considering that both its LUMO and HOMO orbitals look systematically translated to lower values, an effect that might be linked to interactions with the long alkyl chain in the DFT vacuum conditions.

Thus, overall, the present series features, according to both CV experiments and DFT calculations, HOMO-LUMO gaps not lower, but even higher than the parent compound. It is also worthwhile noting that electrochemical and DFT gap values look close, although of course they are not expected to coincide given the different conditions. It is also interesting to note that in the present series, and especially in the **2**[12] and **3** terms, the twin peak potential difference is significantly lower with respect to parent case without phenyl linker. This feature could point to lower interaction between equivalent redox sites on account of less convenient reciprocal positions of the two moieties in space.

Implementation of Inherently Chiral Selectors as Electrode Surfaces or Ionic Liquid Additive

To prepare chiral electrode surfaces for the subsequent enantiodiscrimination experiments, oligomer films were electrodeposited in CH_2Cl_2 from monomers **1** and **2** by repeated potential cycling around the potential corresponding to the third oxidation peak, i.e. the first one involving the bithiophene wings with free terminals (as discussed in the former paragraph). Similarly to the parent case,[1] electrooligomerization of **1** and **2**,[12] that should follow the usual thiophene electrooligomerization scheme,[31] proceeds fast (Figure SI.4 left) and the grown oligomer films (**oligo-1** and **oligo-2** respectively) show good stability upon subsequent potential cycling in monomer-free solution (Figure SI.4 right), a treatment performed in order to eliminate monomer residuals and to check the film stability in repeated doping/undoping cycles, as required for use as enantioselective electrode surfaces.

Instead no significant film formation can be achieved by applying the same protocol to monomer **3** (Figure SI.4 last line), very likely as a consequence of the high solubility originating from the very long alkyl chains; for this reason, **3**, unlike **1** and **2**, was tested as chiral additive in achiral ionic liquid (see later on).

Voltammetry enantiodiscrimination experiments

Selectors implemented as inherently chiral oligomer film electrode surfaces: Voltammetry experiments were carried out on GC electrodes modified with the above electrodeposited electroactive oligomer films in both enantiopure configurations, comparing the features of (*S*)- and (*R*)-enantiomers of two chiral electroactive probes (Figure 8):

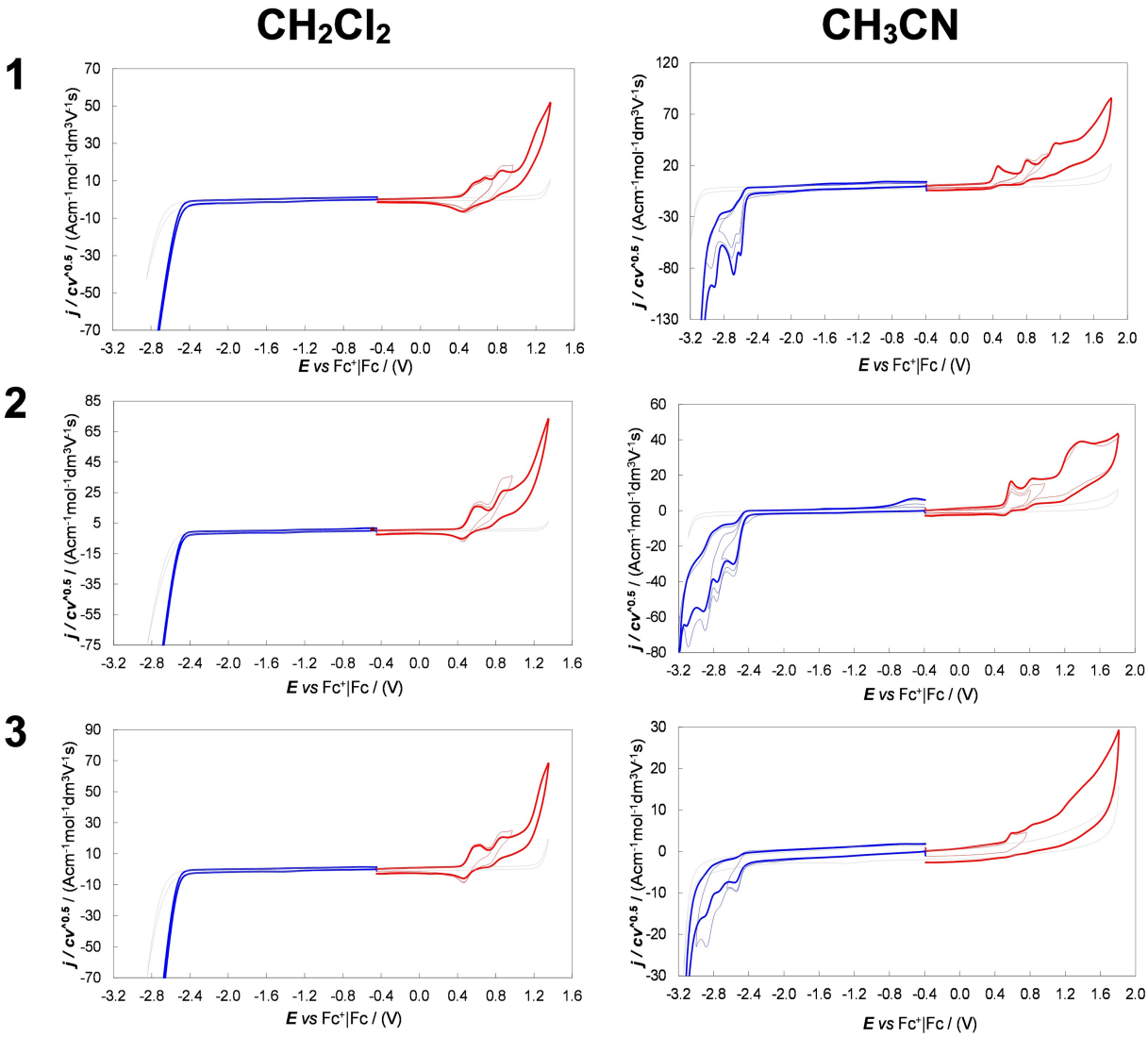

Figure 7. Normalized CV patterns, assembled from first oxidation and first reduction half cycles in order to exclude possible interferences from reciprocal reaction products, obtained for 0.00075 M **1**, **2** and **3** in CH_3CN (right side) and CH_2Cl_2 (left side) with 0.1 M $TBAPF_6$ supporting electrolyte, on GC electrode, at 0.2 V s^{-1}. Background patterns are also reported in grey, for sake of comparison.

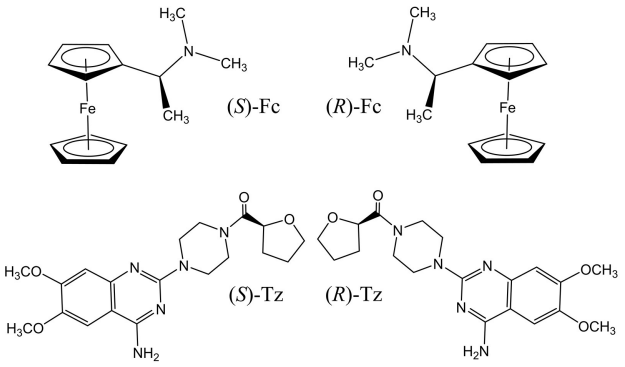

Figure 8. The enantiomers of two electroactive chiral probes.

a) *N,N'*-dimethyl-1-ferrocenylethylamine (**(*S*)-Fc**, **(*R*)-Fc**), our standard electroactive chiral probe, commercially available and featuring a chemically and electrochemically first CV oxidation peak in a potential range close to the parent Fc one, i.e. close to O V vs. $Fc^+|Fc$) at which the chiral oligomer film is still practically uncharged (Figure SI.4);

b) terazosin ([4-(4-amino-6,7-dimethoxy-quinazolin-2-yl) piperazin-1-yl]-tetrahydrofuran-2-yl-methanone; **(*S*)-Tz**, **(*R*)-Tz**), an active pharmaceutical ingredient (API) currently applied to treatment of high blood pressure and prostatic hyperplasia, featuring a chemically and electrochemically irreversible first CV oxidation peak (Figure SI.5), possibly corresponding to the oxidation of the methylated cathecolic ring, in a potential range at which the chiral oligomer film is positively charged. (Figure SI.4)

Very good enantiodiscrimination in terms of DPV peak potential differences is obtained for the **(*S*)-Fc** and **(*R*)-Fc** enantiomers on **oligo-1** enantiopure films, resulting in a peak potential difference of about 160 mV, a large one, although

Table 3. Selected parameters from the CV features of monomers **1,2,3** and parent monomer **2,2′-(N-Me-IND)$_2$-T$_4$**, in CH_2Cl_2 and in CH_3CN, with 0.1 M $TBAPF_6$ as supporting electrolyte, with related estimated energy parameters (Supporting Information.3).

		CV peaks									
		III c	II c	I c	I a	II a	III a	IV a			
Monomer	Solvent	E_p/V(Fc$^+$|Fc) 0.2 (2) V s^{-1}	E_p/V(Fc$^+$|Fc) 0.2 (2) V s^{-1}	E_p/V(Fc$^+$|Fc) 0.2 (2) V s^{-1}	E_p /V(Fc$^+$|Fc) 0.2 (2) V s^{-1}	E_p/V(Fc$^+$|Fc) 0.2 (2) V s^{-1}	E_p/V(Fc$^+$|Fc) 0.2 (2) V s^{-1}	E_p/V(Fc$^+$|Fc) 0.2 (2) V s^{-1}	LUMO/eV	HOMO/eV	HL gap/eV
2,2′-(N–Me-IND)$_2$T$_4$	DCM				0.36 (0.37)	0.53 (0.54)	0.75 (0.78)	0.87 (0.92)		−5.16	
	ACN	−2.94	−2.70	−2.62	0.47 (0.48)	0.58 (0.61)	0.81 (0.84)	0.98 (1.03) 1.16 (1.18)	−2.18	−5.27	3.09
2,2′-(N–Me-IND)$_2$Ph$_2$T$_4$ 1	DCM				0.56 (0.57)	0.67 (0.70)	0.81 (0.82)			−5.36	
	ACN	−2.91	−2.68	−2.61^{shoulder}	0.48 (0.50)	n.d. (0.59)	0.82 (0.84)	0.98 (1.03)	−2.19	−5.28	3.09
2,2′-(N–Pr-IND)$_2$Ph$_2$T$_4$ 2	DCM				0.58 (0.64)	0.65 (0.70)	0.86 (0.90)			−5.38	
	ACN	−2.91 (2.94), −3.14 (3.15)	−2.77 (2.83)	−2.56 (2.57)	0.59 (0.64)	0.82 (0.84)	1.36 (1.40)		−2.24	−5.39	3.15
2,2′-(N-Hex-IND)$_2$Ph$_2$T$_4$ 3	DCM				0.57 (0.59)	0.64 (0.70)	0.85 (0.87)			−5.37	
	ACN	−2.88 (2.92)	−2.74 (2.77)	−2.57 (2.59)	0.60 (0.62)	0.85	1.24		−2.23	−5.40	3.17

lower respect to the ~350 mV one observed in the same conditions in the cited parent case of **(N-Me-IND)$_2$-T$_4$**[1] without phenyl spacer. On **oligo-2** the difference is smaller, about 80 mV, pointing to less effective enantiodiscrimination, that is however still significant and reproducible. Notably, the same probe/selector enantiomer combination order is observed in both cases, i.e. with the *S,R* (or specularly *R,S*) combination preceding the *S,S* (or specularly *R,R*) one. (Figure 9)

This is indeed consistent with enantioselectivity arising from the same atropisomeric bisindole scaffold.

As in previous cases, such potential differences between probe enantiomers, concerning a chemically and electrochemically reversible electron transfer process, should correspond to the thermodynamic energy difference for the diastereomeric probe/selector combinations obtained testing the two enantiomers with the same selector configuration (or *vice versa*). In fact, some coordination could be assumed between probe and selector, at least moderate/transient, and rather wide-scope than specific, hinging on the many involved π systems and heteroatoms; and such coordination could be significantly more effective for one combination with respect to the other one.

Actually, consistently with the well-known treatment by Kolthoff and Lingane for electroactive species undergoing reversible electron transfer,[32] coordination results in a formal potential shift (in negative or positive direction depending on the process being a reduction or oxidation, and on the species most stabilized by coordination being the reagent or product one) of $(k/n)\log K$, where K is the coordination equilibrium constant.

Thus, even mild coordination with $K \sim 10/10^2/10^3$, or a $\sim 10/10^2/10^3$ coordination constant ratio for diastereomeric situations, would justify a shift/difference of 60/120/180 mV in peak potential for a species undergoing monoelectronic reversible process. In the light of this, the smaller peak potential difference in the **oligo-2** case should point to less effective coordination and/or smaller differentiation in coordination ability, linked to the perturbing presence of the long aliphatic chains, more likely than to the chiral film being possibly thinner (Figure SI.4). Concerning peak currents, they are notably lower than on the bare electrode; this looks consistent with the neutral state of the oligomer film, implying that the probe can only react diffusing inside the film to the GC electrode surface;[33] this could be easier in the case of **oligo-2**, possibly resulting in the same conditions in a thinner film, as already mentioned, which could justify the higher currents with respect to the **oligo-1** case.

The two chiral probe enantiomers were also successfully discriminated when simultaneously present, either in 1:1 ratio (racemic **(±)-Fc**) or in asymmetric ratios (Figure 10 (a) and (b), respectively). In all cases two neatly separated peaks, located at potentials close to the single enantiomer ones are observed. Moreover, the peak current ratios for the two enantiomers appear to be consistent with their concentration ratios, pointing to the possibility of direct evaluation of enantiomeric excesses from the CV pattern analysis.

CV tests in aqueous buffer with the enantiomers of chiral probe terazosin, undergoing irreversible electron transfer at the

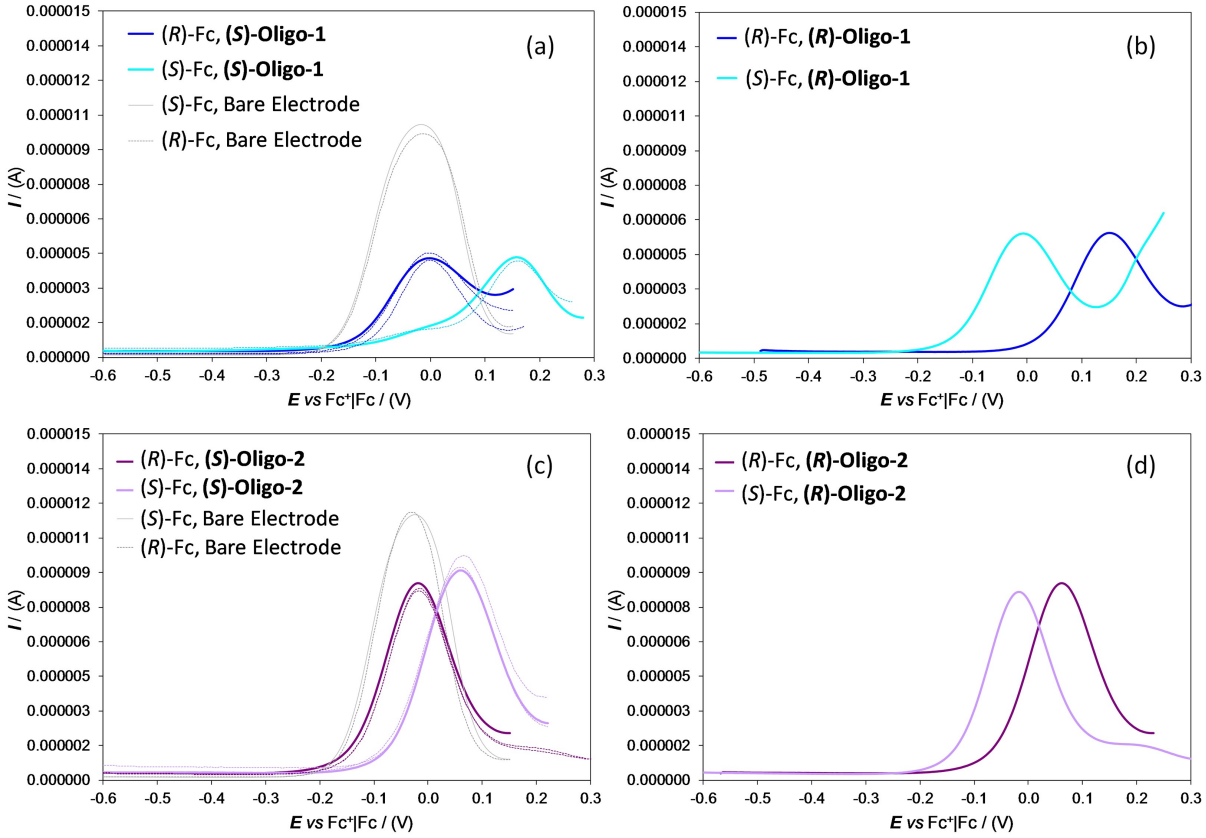

Figure 9. Enantiodiscrimination performances of enantiopure (a) (***S***)-**oligo-1** and (b) (***R***)-**oligo-1** and of (c) (***S***)-**oligo-2** and (d) (***R***)-**oligo-2** electrode surfaces towards 0.002 M (*S*)- and (*R*)-Fc probes in CH_2Cl_2 + 0.1 M $TBAPF_6$. Patterns recorded for the two enantiomers on bare GC are also reported in grey.

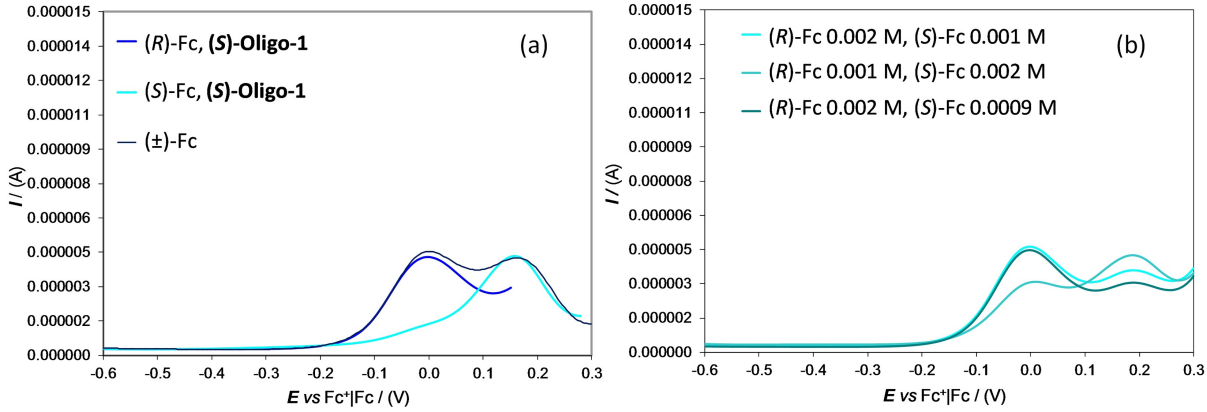

Figure 10. Enantiodiscrimination performances of enantiopure (***S***)-**oligo-1** towards the ferrocenyl probe enantiomers simultaneously present (a) in 1 : 1 ratio (racemate, (±)-**Fc**); (b) in different ratios.

chiral film oxidation onset ($E_{p,a}$ about 0.96 V vs. SCE), result in smaller but still significant and reproducible peak potential differences, of about 80 mV vs. SCE on **oligo-1** and about 40 mV on **oligo-2**, specularly inverting selector or probe configuration. (Figure 11)

Notably, again the enantiodiscrimination is less effective for the selector with longer alkyl chains. Concerning currents, they again exhibit a linear dynamic range for the probe enantiomer concentrations, but in this case they appear comparable or even higher respect to those recorded on bare electrode. This feature looks consistent with the whole film having become conductive and thus potentially acting as electrode.[33]

Selector implemented as inherently chiral additive in ionic liquid: The enantiodiscrimination ability of monomer **3**, unsuit-

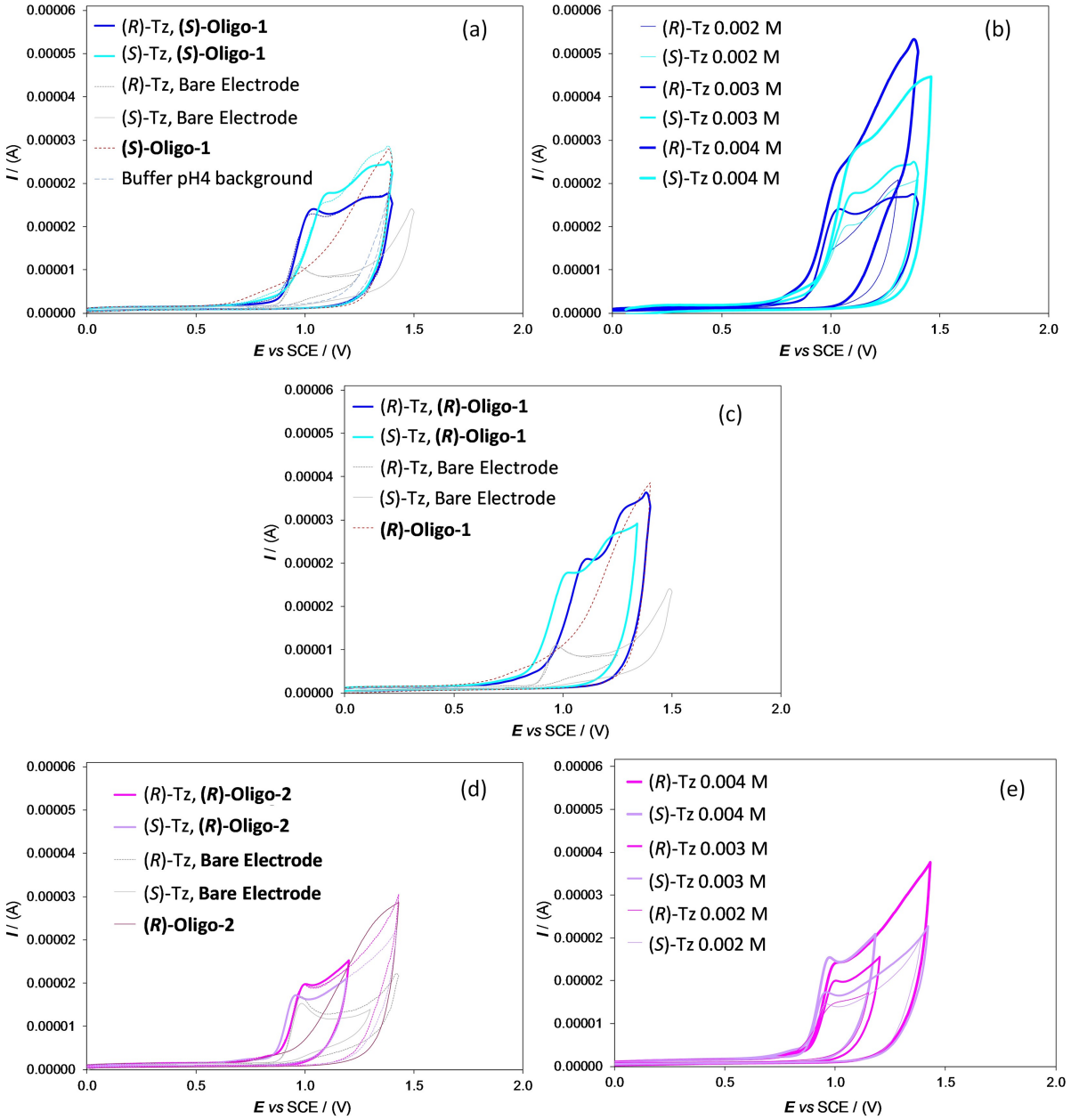

Figure 11. Enantiodiscrimination performances of enantiopure a),b) (***S***)-**oligo-1**; c) (***R***)-**oligo-1**; d),e) (***R***)-**oligo-2** electrode surfaces towards (***S***)- and (***R***)-**Tz** probes (0.002 M in a,c,d) in aqueous pH 4 buffer. For sake of comparison, patterns are also reported for the film oxidation onset in the absence of the probe (red dotted thin lines) and for the two enantiomers on bare GC (grey lines).

able for electrooligomerization, was tested employing it as chiral additive in achiral ionic liquid 1-butyl-3-methylimidazolium bis(trifluoromethylsulfonyl) imide BMIMTf$_2$, according to our alternative recently developed enantiodiscrimination strategy which exploits the high and modulable local order of ionic liquid media at the electrochemical interphase.[8,13] In this case CV tests were performed with (***R***)-**Fc** and (***S***)-**Fc** probes in very thin solution layers on screen printed graphite working electrodes, resulting in a potential difference for the two enantiomers even larger (about 230 mV) than that obtained for the same probes on **oligo-1** films in CH_2Cl_2 + 0.1 M $TBAPF_6$ (Figure 12).

Conclusion

The family of inherently chiral electroactive selectors (**N-R-IND)$_2$-Ph$_2$-T$_4$**, based on the 2,2′-biindole atropisomeric scaffold with 2,2′-bithiophene terminals connected to the core through a phenyl ring can be easily synthesized and has modulable functional properties. Our chiral HPLC protocols, optimized

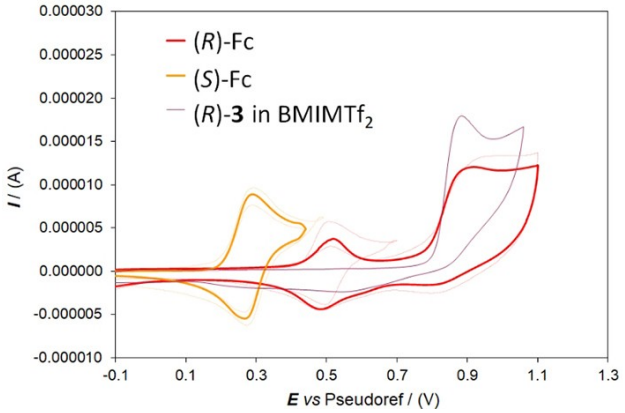

Figure 12. Enantiodiscrimination performances of enantiopure (***R***)-**3** (employed as chiral additive in $BMIMTf_2$, at 0.01 M) towards (*S*)- and (*R*)-Fc probes (0.002 M). For sake of comparison, the CV pattern is also reported for the monomer oxidation in the absence of the probe (purple thin lines).

through a careful study as a function of molecular structure, temperature, as well as eluent mixture, enable excellent semi-preparative resolution into antipodes, apparently enhanced with respect to the parent **(N-Me-IND)$_2$-T$_4$** case by the presence of the phenyl spacer.

The enantiomers thus obtained have remarkable chiroptical features, in terms of optical rotation as well as circular dichroism, consistently with the presence of an atropisomeric chromophore. Their electronic features are similar to parent **(N-Me-IND)$_2$-T$_4$**, the phenyl spacer resulting in a slightly larger HOMO-LUMO gap on account of slightly less efficient conjugation with the biindole core where the first oxidation process is localized.

In any case, the present series shows good performances when applied as selectors in chiral voltammetry for discrimination of the enantiomers of model chiral ferrocenyl probes, either in CH_2Cl_2, by conversion into enantiopure electroactive electrode surfaces by electrooligomerization on glassy carbon substrate (monomers **1** and **2**), or in achiral ionic liquid $BMIMTf_2$, as chiral additive (monomer **3** with hexyl chains, which hamper electrooligomerization). Discrimination is conveniently and reproducibly achieved in terms of significant potential differences for the two enantiomers, specularly inverting either probe or selector configuration. In one case, successful discrimination is even observed with the two probe enantiomers concurrently present, either as racemate or with enantiomeric excesses, neatly accounted for by the peak current ratios.

Oligo-1 and **oligo-2** films also result in enantiomer discrimination for a quite different chiral probe, active pharmaceutical ingredient terazosin, working in aqueous buffer, confirming the wide-scope effectiveness of the chiral selectors and suggesting application to a wider pool of chiral probes of applicative interest. At the same time, the systematic chiral selector series now available can also be regarded as a useful tool to investigate probe/selector interactions to achieve rational criteria for optimization of selector design and management.

Experimental Section

Monomer synthesis

Chemicals and Reagents

All reactions were performed with oven-dried laboratory glassware, under nitrogen atmosphere unless otherwise indicated. All reactants and dry solvents were purchased from Sigma Aldrich, Tokyo Chemical Industry and Fluorochem, and used as received. TLC analysis were performed on ALUGRAM® Xtra SIL G/UV254 (0.2 mm thin layer depth; Macherey-Nagel). Gravimetric chromatography columns were performed using silica gel (particles diameter: 0.63–2.00 mm) as stationary phase. ^{1}H NMR spectra (chapter SI.1 in the Supporting Information) were recorded with Bruker AVANCE instrument operating at 400.13 MHz with TMS as internal standard. ^{13}C NMR spectra (chapter SI.1) were recorded at 100.56 MHz with total proton decoupling with TMS as internal standard. Mass analyses were performed by using a VG 7070 EQ-HF instrument.

Synthesis of 6: 5-(4-Bromophenyl)-2,2′-bithiophene (**5**) (200 mg, 0.623 mmol), potassium carbonate (133 mg, 0.965 mmol) and Pd-$(PPh_3)_4$ (22 mg, 0.019 mmol) were added at r.t. to a solution of butadiine **4** (82 mg, 0.193 mmol) in MeCN (7 mL). Reaction mixture was refluxed for 3 h then diluted with water, extracted with DCM, dried over $MgSO_4$. After removal of the solvent under reduced pressure, the product was purified through gravimetric column chromatography (DCM/*n*-hexane 2:1) to afford compound **6** (50 mg, 36%) as a yellow solid. ^{1}H NMR (400 MHz, DMSO-d_6) δ: 11.69 (s, 2H), 7.70 (d, J=8 Hz, 2H), 7.52 (d, J=4 Hz, 2H), 7.46-7.44 (m, 4H), 7.38 (d, J=4 Hz, 2H), 7.31 (d, J=4 Hz, 2H), 7.28 (d, J=4 Hz, 2H), 7.24-7.19 (m, 6H), 7.14-7.09 (m, 6H). ^{13}C NMR (100 MHz, DMSO-d6) δ: 142.3, 136.5, 136.4, 135.2, 134.4, 130.4, 129.0, 128.3, 126.9, 126.4, 125.4, 125.0, 125.0, 124.0, 123.8, 122.3, 118.9, 115.3, 111.8. MS (EI): 712 (100%). m.p.: 299 °C (decomposition).

General procedure for alkylation: KOH (0.8 mmol) was added to a solution of **6** (0.16 mmol) in DMF (5 mL), and reaction mixture was stirred at r.t. for 0.5 h. Then the suitable alkylating agent (2.4 mmol) was added and the reaction mixture stirred for 48 h. Solvent was removed under reduced pressure and the product purified by gravimetric column chromatography using as eluent a 8:2 *n*-hexane/ AcOEt mixture.

Synthesis of compound 1

Iodomethane was employed as alkylating agent; 98% yields. ^{1}H NMR (DMSO-d_6): 7.93 (d, J=8 Hz, 2H), 7.65 (d, J=8 Hz, 6H), 7.56 (d, J=4 Hz, 2H), 7.51 (d, J=4 Hz, 2H)7-39-7.33 (m, 10H), 7.32 (t, J=8 Hz, 2H), 7.16 (t, J=4 Hz, 2H), 3.48 (s, 6H); ^{13}C NMR (100 MHz, DMSO-d6) δ: 141.8, 137.4, 136.3, 135.5, 134.1, 130.7, 128.3, 128.3, 127.3, 125.5, 125.4, 125.4, 125.1, 124.4, 124.0, 122.8, 120.5, 119.3, 116.9, 110.7, 30.3.

Synthesis of compound 2:[12] 1-Bromopropane was employed as alkylating agent; 95% yield. ^{1}H NMR ($CDCl_3$) δ: 7.94 (d, J=8 Hz, 2H), 7.42 (d, J=8 Hz, 4H), 7.36 (d, J=8 Hz, 4H), 7.28 (d, J=8 Hz, 2H), 7.25 (t, J=8 Hz, 2H), 7.21 (m, 2H), 7.14 (d, J=4 Hz, 2H), 7.10 (m, 4H), 7.04 (d, J=4 Hz, 2H), 6.94 (t, J=4 Hz, 2H), 3.72 – 3.65 (m, 2H), 3.69 – 3.59 (m, 2H), 1.19 – 1.04 (m, 4H), 0.60 (t, J=8 Hz, 6H) ppm.^{13}C NMR ($CDCl_3$) δ: 143.1, 137.5, 137.1, 136.3, 134.5, 131.5, 128.6, 128.9, 127.1, 126.4, 125.8, 124.6, 124.3, 123.5, 123.3, 122.7, 120.4, 120.2, 117.7, 110.7, 45.8, 22.7, 11.5 ppm. MS (ESI): 797 [M$^+$], 798 [M+1].

Synthesis of compound 3: 1-Bromohexane was employed as alkylating agent; 92% yield. ^{1}H NMR (400 MHz, DMSO-d_6) δ: 7.96 (d, J=8 Hz, 2H), 7.93 (d, J=8 Hz, 4H), 7.57 (d, J=8 Hz, 2H), 7.52-7.44

(m, 8H), 7.31-7.23 (m, 8H), 7.10 (t, $J=8$ Hz, 2H), 3.85-3.71 (m, 4H), 1.22 (br, 2H), 1.00-0.85 (m, 14H), 0.64 (t, $J=8$ Hz, 6H). ^{13}C NMR (100 MHz, $CDCl_3$) δ: 143.1, 137.6, 137.1, 136.3, 134.5, 131.5, 128.6, 127.9, 127.2, 126.4, 125.9, 124.6, 124.3, 123.5, 123.3, 122.7, 120.4, 120.2, 117.8, 110.7, 44.2,31.1, 29.4, 26.7, 22.4, 13.9. MS (EI): 881 (100%). m.p.: 104–105 °C.

Theorical computations of monomer features

Preliminary energy structures were obtained by MonteCarlo conformational analysis performed with Molecular Mechanics calculations using the OPLS 2005 force field[34] of the Macromodel[35] package in the Schrödinger suite,[36] since many conformers are possible due to the mobility of the aromatic pendant groups. In this way, the best arrangement for the different substituents around the 2,2′-biindole scaffold was obtained. According to force field analysis, compounds **1,2,3** in their most stable conformation presents the two thiophene rings oriented in a trans arrangement. These conformations have been employed as initial structures to calculate the racemization barrier by PM6 semi-empirical method[37] and by DFT approach using Gaussian G09 rev E.01 package.[38] The transition states responsible of the interconversion of the two enantiomers (*S*)Δ(*R*), were fully optimized to the relative genuine TSs (each with only one imaginary frequency), using B3LYP[39] functional with 6-31G(d,p) basis set. These geometries have been then employed in a single point energy calculations at B3LYP/6-311 + G(3df,3pd) level of theory in order to obtain information related to HOMO-LUMO orbitals.

Enantioselective HPLC

HPLC-grade solvents were supplied by Aldrich (Milan, Italy). HPLC enantioseparations were performed by using stainless-steel Chiralpak® IB 250 mm × 4.6 mm and 250 mm × 10 mm columns (Chiral Technologies Europe, Illkirch-Graffenstaden, France). The analytical HPLC system consisted of a PerkinElmer 200 LC pump equipped with a Rheodyne injector, a 50 μL sample loop, an HPLC Dionex CC-100 oven and a Jasco Model CD 2095 Plus UV/CD detector. For semi-preparative enantioseparations, a PerkinElmer 200 LC pump equipped with a Rheodyne injector, a 5 mL sample loop, a PerkinElmer LC 101 oven and Waters 484 detector were used. The signal was acquired and processed by the Clarity software of DataApex.

During semipreparative HPLC of **1**–**3** two fractions corresponding to the enantiomeric peaks of racemic mixture were pooled. Evaporation of pooled fractions yielded a yellow solid. The enantiomeric excess (ee) of the collected enantiomers was evaluated by HPLC using the analytical Chiralpak IB 250 mm × 4.6 mm column and the same mobile phase employed in the mg-scale resolution (*n*-hexane-dichloromethane-ethanol 100:5:1 (v/v/v)). The enantiomers of terazosin (**Tz**) were obtained according to a semipreparative HPLC method previously described.[40] The CD spectra of the enantiomers collected on a semipreparative scale were recorded in chloroform at 25 °C by using a Jasco Model J-700 spectropolarimeter. The optical path was 1 mm. The spectra are average computed over three instrumental scans and the intensities are presented in terms of ellipticity values (mdeg). Specific rotations were measured by a PerkinElmer polarimeter model 241 equipped with Na/Hg lamps. The volume of the cell was 1 mL and the optical path was 10 cm. The system was set at a temperature of 20 °C.

Electrochemistry

Preliminary electrochemical characterization of inherently chiral monomers 1, 2 and 3: Cyclic voltammetry (CV) and Differential Pulse Voltammetry (DPV) experiments were performed using an Autolab PGSTAT potentiostat (Eco-Chemie, Utrecht, The Netherlands), controlled by a PC with the GPES software provided by the same manufacturer. The three-electrode V-shaped minicell (with 3 cm^3 of solution) included a glass-embedded glassy carbon disk (GC, Metrohm, $S=0.033$ cm^2) as working electrode, a Pt disk as counter electrode, and an aqueous saturated calomel (SCE) as reference electrode, inserted in a compartment filled with the working medium and ending with a porous frit, to avoid water and KCl leakage into the working solution. The optimized preliminary polishing procedure for the GC disk electrode consisted in treatment with a diamond powder of 1 μm diameter (Aldrich) on a wet DP-Nap cloth (Struers). The CV characterizations of **1,2,3** were performed at scan rates in the 0.05-2 $V\,s^{-1}$ range, on 0.00075 M probe solutions in both acetonitrile (CH_3CN, Aldrich, HPLC grade), and dichloromethane (CH_2Cl_2, Aldrich, HPLC grade) with 0.1 M tetrabutylammonium hexafluophosphate ($TBAPF_6$) as supporting electrolyte (Fluka, ≥98%), applying ohmic drop compensation by the positive feedback method and referring the potentials to the $Fc^+|Fc$ redox couple (the intersolvental standard recommended by IUPAC[41]) measured in the same conditions (~0.39 V vs. SCE in CH_3CN and ~0.49 V vs. SCE in CH_2Cl_2).

Electrode modification by electrodeposition of the oligo-1 and oligo-2 chiral films: Electrodepositions of enantiopure electroactive oligomer chiral films **oligo-1** and **oligo-2** on the GC disk electrode were performed from 0.00075 M solutions of the corresponding enantiopure **1** or **2** monomers, by 36 repeated CV cycles around the potential corresponding to the third oxidation peak, at 0.05 $V\,s^{-1}$ scan rate, in CH_2Cl_2 solvent with 0.1 M $TBAPF_6$ supporting electrolyte.

Enantiodiscrimination experiments

a) DPV tests with ferrocenyl probes on uncharged **oligo-1** and **oligo-2** films. A first series of enantiodiscrimination experiments were performed in the above minicell, by Differential Pulse Voltammetry (DPV; step potential 4 mV, modulation amplitude 50 mV) using the enantiomers of *N,N′*-dimethyl-1-ferrocenylethylamine as chiral probes, at 0.05 $V\,s^{-1}$ scan rate in 0.002 M solutions of the probe in $CH_2Cl_2 + TBAPF_6$ 0.1 M as supporting electrolyte. Reproducibility tests were performed by repeatedly recording the DPV patterns of model probes on freshly deposited chiral surfaces.

b) CV tests with terazosin probes on positively charged **oligo-1** and **oligo-2** films. A second series of enantiodiscrimination tests were performed in the above minicell, by cyclic voltammetry (CV) at 0.05 $V\,s^{-1}$ scan rate with the enantiomers of terazosin as 0.003 M chiral probes in commercial pH 4 buffer (Fluka, prepared with citric acid, NaOH, and NaCl). In this case the optimized conditions for electrooligomerization were 20 CV cycles at 0.2 $V\,s^{-1}$. Again, reproducibility tests were performed by repeatedly recording the CV patterns of model probes on freshly deposited chiral surfaces.

c) CV tests with ferrocenyl probes in achiral ionic liquid with **3** chiral additive. A third series of CV tests was carried out with the enantiomers of *N,N′*-dimethyl-1-ferrocenylethylamine as chiral probes, in a drop of achiral ionic liquid $BMIMTf_2$ with 0.01 M **3** as chiral additive, using screen-printed electrode cells constituted of working, counter, and Ag/AgCl pseudoreference electrodes. The electrodes were produces in foils of 48 using screen-printing machine DEK 245 (Weymouth, UK) and flexible

polyester film (Autostat HT5) as support obtained from Autotype Italia (Milan, Italy). Graphite-based ink (Elettrodag 421) from Acheson (Milan, Italy) was used to print the working and the counter electrode while silver/silver chloride ink was used to print the reference electrode (Acheson Elettrodag 4038 SS). The diameter of the SPE working electrode was 0.4 cm resulting in an apparent geometric area of 0.126 cm^2.

Acknowledgements

Fondazione Cariplo and Regione Lombardia as well as Università degli Studi di Milano are acknowledged for support to the chiral electroanalysis research group in Milano. Rossella Monaco is also acknowledged for some preliminary CV experiments.

Conflict of Interest

The authors declare no conflict of interest.

Keywords: additives · chiral · enantioselective HPLC · electrochemistry · electrodes · oligomers

[1] S. Arnaboldi, T. Benincori, A. Penoni, L. Vaghi, R. Cirilli, S. Abbate, G. Longhi, G. Mazzeo, S. Grecchi, M. Panigati, P. R. Mussini, *Chem. Sci.* **2019**, *10*, 2708–2717.
[2] S. Arnaboldi, S. Grecchi, M. Magni, P. Mussini, *Curr. Opin. Electrochem.* **2018**, 7, 188–199.
[3] N. Berova, L. Di Bari, G. Pescitelli, *Chem. Soc. Rev.* **2007**, 36, 914–931.
[4] J. T. Vázquez, *Tetrahedron: Asymmetry* **2017**, *28*, 1199–1211.
[5] S. Arnaboldi, M. Magni, P. Mussini, *Curr. Opin. Electrochem.* **2018**, *8*, 60–72.
[6] F. Sannicolò, S. Arnaboldi, T. Benincori, V. Bonometti, R. Cirilli, L. Dunsch, W. Kutner, G. Longhi, P. R. Mussini, M. Panigati, M. Pierini, S. Rizzo, *Angew. Chem. Int. Ed.* **2014**, *53*, 2623–2627; *Angew. Chem.* **2014**, *126*, 2661–2665.
[7] S. Arnaboldi, T. Benincori, R. Cirilli, W. Kutner, M. Magni, P. R. Mussini, K. Noworyta, F. Sannicolò, *Chem. Sci.* **2015**, *6*, 1706–1711.
[8] S. Rizzo, S. Arnaboldi, V. Mihali, R. Cirilli, A. Forni, A. Gennaro, A. A. Isse, M. Pierini, P. R. Mussini, F. Sannicolò, *Angew. Chem. Int. Ed.* **2017**, *56*, 2079–2082; *Angew. Chem.* **2017**, *129*, 2111–2114.
[9] F. Sannicolò, P. R. Mussini, T. Benincori, R. Cirilli, S. Abbate, S. Arnaboldi, S. Casolo, E. Castiglioni, G. Longhi, R. Martinazzo, M. Panigati, M. Pappini, E. Quartapelle Procopio, S. Rizzo, *Chem. Eur. J.* **2014**, *20*, 15298–15302.
[10] F. Sannicolò, P. R. Mussini, T. Benincori, R. Martinazzo, S. Arnaboldi, G. Appoloni, M. Panigati, E. Quartapelle Procopio, V. Marino, R. Cirilli, S. Casolo, W. Kutner, K. Noworyta, A. Pietrzyk-Le, Z. Iskierko, K. Bartold, *Chem. Eur. J.* **2016**, *22*, 10839–10847.
[11] G. Bonetti, S. Arnaboldi, S. Grecchi, G. Appoloni, E. Massolo, S. Rossi, R. Martinazzo, F. Orsini, P. R. Mussini, T. Benincori, *Molecules* **2020**, *25*, 2175.
[12] C. Malacrida, L. Scapinello, R. Cirilli, S. Grecchi, A. Penoni, T. Benincori, S. Ludwigs, *ChemElectroChem* **2021**, 8, 1–13.
[13] S. Rizzo, S. Arnaboldi, R. Cirilli, A. Gennaro, A. A. Isse, F. Sannicolò, P. R. Mussini, *Electrochem. Commun.* **2018**, *89*, 57–61.
[14] G. Abbiati, A. Arcadi, E. Beccalli, G. Bianchi, F. Marinelli, E. Rossi, *Tetrahedron* **2006**, *62*, 3033–3039.
[15] M. G. Saulnier, D. B. Frennesson, M. S. Deshpande, D. M. Vyas, *Tetrahedron Lett.* **1995**, *36*, 7841–7844.
[16] C. I. Lin, S. Selvi, J. M. Fang, P. T. Chou, C. H. Lai, Y. M. Cheng, *J. Org. Chem.* **2007**, *72*, 3537–3542.
[17] W. Lee, N. Cho, J. Kwon, J. Ko, J. I. Hong, *Chem. Asian J.* **2012**, *7*, 343–350.
[18] L. D. Asnin, M. V. Stepanova, *J. Sep. Sci.* **2018**, *41*, 1319–1337.
[19] R. Cirilli, M. R. Del Giudice, R. Ferretti, F. La Torre, *J. Chromatogr. A* **2001**, *923*, 27–36.
[20] M. Pierini, S. Carradori, S. Menta, D. Secci, R. Cirilli, *J. Chromatogr. A* **2017**, *1499*, 140–148.
[21] A. Sepsey, É. Horváth, M. Catani, A. Felinger, *J. Chromatogr. A* **2020**, *1611*, 460594.
[22] S. Rizzo, S. Menta, C. Faggi, M. Pierini, R. Cirilli, *J. Chromatogr. A* **2014**, *1363*, 128–136.
[23] M. Kazusaki, Y. Ohgami, *Chromatographia* **2007**, *28*, 125–130.
[24] C. Panella, R. Ferretti, A. Casulli, R. Cirilli, *J. Pharm. Anal.* **2019**, *9*, 324–331.
[25] I. Matarashvili, G. Kobidze, A. Chelidze, G. Dolidze, N. Beridze, G. Jibuti, T. Farkas, B. Chankvetadze, *J. Chromatogr. A* **2019**, *1599*, 172–179.
[26] T. Benincori, G. Appoloni, P. R. Mussini, S. Arnaboldi, R. Cirilli, E. Quartapelle Procopio, M. Panigati, S. Abbate, G. Mazzeo, G. Longhi, *Chem. Eur. J.* **2018**, *24*,11082–11093.
[27] A. J. Bard, L. R. Faulkner, *Electrochemical Methods: Fundamentals and Applications*, II ed., Wiley, New York, **2001**, pp. 505–509.
[28] G. Di Carlo, A. Orbelli Biroli, F. Tessore, M. Pizzotti, P. R. Mussini, A. Amat, F. De Angelis, A. Abbotto, V. Trifiletti, R. Ruffo, *J. Phys. Chem. C* **2014**, *118*, 7307–7320.
[29] M. I. Nan, E. Lakatos, G. I. Giurgi, L. Szolga, R. Po, A. Terec, S. Jungsuttiwong, I. Grosu, J. Roncali, *Dyes Pigm.* **2020**, *181*, 108527.
[30] L. Zhang, N. S. Colella, B. P. Cherniawski, S. C. B. Mannsfeld, A. L. Briseno, *ACS Appl. Mater. Interfaces* **2014**, *6*, 5327–5343.
[31] J. Heinze, B. A. Frontana-Uribe, S. Ludwigs, *Chem. Rev.* **2010**, *110*, 4724–4771
[32] I. M. Kolthoff, J. J. Lingane, *Polarography*, Vol. 1 (2nd Ed.), Interscience, New York, **1952**, pp. 189–234.
[33] M. Donnici, R. Toniolo, S. Arnaboldi, P. R. Mussini, T. Benincori, R. Cirilli, S. Daniele, *Molecules* **2020**, *25*, 5368–5383.
[34] G. A. Kaminski, R. A. Friesner, J. Tirado-Rives, W. L. Jorgensen, *J. Phys. Chem. B* **2001**, *105*, 6474–6487.
[35] MacroModel, version 11.2, Schrödinger, LLC, New York, NY, **2016**.
[36] Small-Molecule Drug Discovery Suite 2016-4, Schrodinger, LLC, New York, NY, **2016**.
[37] J. J. P. Stewart, *J. Mol. Model.* **2007**, *13*, 1173–1213.
[38] M. J. Frisch, G. W. Trucks, H. B. Schlegel, G. E. Scuseria, M. A. Robb, J. R. Cheeseman, G. Scalmani, V. Barone, B. Mennucci, G. A. Petersson, H. Nakatsuji, M. Caricato, X. Li, H. P. Hratchian, A. F. Izmaylov, J. Bloino, G. Zheng, J. L. Sonnenberg, M. Hada, M. Ehara, K. Toyota, R. Fukuda, J. Hasegawa, M. Ishida, T. Nakajima, Y. Honda, O. Kitao, H. Nakai, T. Vreven, J. A. Montgomery, Jr., J. E. Peralta, F. Ogliaro, M. Bearpark, J. J. Heyd, E. Brothers, K. N. Kudin, V. N. Staroverov, T. Keith, R. Kobayashi, J. Normand, K. Raghavachari, A. Rendell, J. C. Burant, S. S. Iyengar, J. Tomasi, M. Cossi, N. Rega, J. M. Millam, M. Klene, J. E. Knox, J. B. Cross, V. Bakken, C. Adamo, J. Jaramillo, R. Gomperts, R. E. Stratmann, O. Yazyev, A. J. Austin, R. Cammi, C. Pomelli, J. W. Ochterski, R. L. Martin, K. Morokuma, V. G. Zakrzewski, G. A. Voth, P. Salvador, J. J. Dannenberg, S. Dapprich, A. D. Daniels, O. Farkas, J. B. Foresman, J. V. Ortiz, J. Cioslowski, D. J. Fox, Gaussian 09, Revision D.01. Gaussian, Inc., Wallingford CT, **2013**.
[39] V. A. Rassolov, M. A. Ratner, J. A. Pople, P. C. Redfern, L. A. Curtiss, *J. Comb. Chem.* **2001**, *22*, 976–984.
[40] R. Ferretti, B. Gallinella, F. La Torre, L. Zanitti, L. Turchetto, A. Mosca, R. Cirilli, *J. Chromatogr. A* **2009**, *1216*, 53–5390.
[41] G. Gritzner, J. Kuta, *Pure Appl. Chem.* **1984**, *56*, 461–466.

Manuscript received: May 7, 2021
Accepted manuscript online: June 25, 2021
Version of record online: August 12, 2021

